AD 745188

HIGH-Z PARTICLE COSMIC-RAY EXPOSURE OF APOLLO 8-14 ASTRONAUTS

E. V. Benton

R. P. Henke

University of San Francisco

TECHNICAL REPORT NO. AFWL-TR-72-5

D D C

RECEIVED

JUL 17 1972

B

June 1972

AIR FORCE WEAPONS LABORATORY
Air Force Systems Command
Kirtland Air Force Base
New Mexico

AFWL-TR-72-5

AIR FORCE WEAPONS LABORATORY
Air Force Systems Command
Kirtland Air Force Base
New Mexico 87117

When US Government drawings, specifications, or other data are used for
any purpose other than a definitely related Government procurement operation,
the Government thereby incurs no responsibility nor any obligation whatsoever,
and the fact that the Government may have formulated, furnished, or in any way
supplied the said drawings, specifications, or other data, is not to be
regarded by implication or otherwise, as in any manner licensing the holder
or any other person or corporation, or conveying any rights or permission to
manufacture, use, or sell any patented invention that may in any way be
related thereto.

DO NOT RETURN THIS COPY. RETAIN OR DESTROY.

HIGH-Z PARTICLE COSMIC-RAY EXPOSURE OF APOLLO 8-14 ASTRONAUTS

E. V. Benton
R. P. Henke
University of San Francisco

TECHNICAL REPORT NO. AFWL-TR-72-5

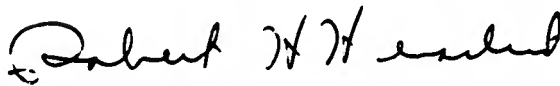Approved for public release; distribution unlimited.

ic

FOREWORD

This report was prepared by the University of San Francisco, San Francisco, California, under Contract F29601-70-C-0077. The research was performed under Program Element 61102F, Project 8803, and was funded by the Office of Aerospace Research.

Inclusive dates of research were November 1969 through December 1971. The report was submitted 14 April 1972 by the Air Force Weapons Laboratory Project Officer, Captain Andrew D. Grimm (SYT).

This report has been reviewed and is approved.

ANDREW D. GRIMM
Captain, USAF
Project Officer

JAY R. ROLAND
Major, USAF
Chief, Theoretical Physics Branch

CARL B. HILLAND
Lt Colonel, USAF
Chief, Technology Division

DOCUMENT CONTROL DATA - R & D

(Security classification of title, body of abstract and indexing annotation must be entered when the overall report is classified)

1. ORIGINATING ACTIVITY (Corporate author)	2a. REPORT SECURITY CLASSIFICATION
University of San Francisco Department of Physics San Francisco, California 94117	Unclassified
	2b. GROUP

3. REPORT TITLE

HIGH-Z PARTICLE COSMIC-RAY EXPOSURE OF APOLLO 8-14 ASTRONAUTS

4. DESCRIPTIVE NOTES *(Type of report and inclusive dates)*

November 1961 through December 1971

5. AUTHOR(S) *(First name, middle initial, last name)*

E. V. Benton, R. P. Henke

6. REPORT DATE	7a. TOTAL NO. OF PAGES	7b. NO. OF REFS
June 1972	44	7

8a. CONTRACT OR GRANT NO. F29601-70-C-0077	9a. ORIGINATOR'S REPORT NUMBER(S)
b. PROJECT NO. 8803	AFWL-TR-72-5
c.	9b. OTHER REPORT NO(S) *(Any other numbers that may be assigned this report)*
d.	

10. DISTRIBUTION STATEMENT

Approved for public release; distribution unlimited.

11. SUPPLEMENTARY NOTES	12. SPONSORING MILITARY ACTIVITY
	AFWL (SYT) Kirtland AFB, NM 87117

13. ABSTRACT

(Distribution Limitation Statement A)

On Apollo missions the individual astronauts' high Z particle exposure was measured by means of Lexan foils located in the passive dosimetry packs carried on the chest, thigh, and ankle of each astronaut. This report deals with measurements obtained on Apollo flights 8-14. Data is presented on the high Z track fluences, the stopping particle densities, and the particle integral LET spectra. The LET spectra, in turn, are used to calculate the fractional cell loss, FCL, of the human kidney (T1) cells arising from the high Z particle exposure. The measurements, on subsequent missions, show a consistent and a significant increase in the observed high Z particle exposure.

DD FORM 1473
1 NOV 65

1a

14. KEY WORDS	LINK A		LINK B		LINK C	
	ROLE	WT	ROLE	WT	ROLE	WT
Dosimetry						
Space radiation						
Solid state detector						
Radiation transport						
Linear energy transfer spectrometer						

ABSTRACT

On Apollo missions the individual astronauts' high Z particle exposure was measured by means of Lexan foils located in the passive dosimetry packs carried on the chest, thigh, and ankle of each astronaut. This report deals with measurements obtained on Apollo flights 8-14. Data is presented on the high Z track fluences, the stopping particle densities, and the particle integral LET spectra. The LET spectra, in turn, are used to calculate the fractional cell loss, FCL, of the human kidney (Tl) cells arising from the high Z particle exposure. The measurements, on subsequent missions, show a consistent and a significant increase in the observed high Z particle exposure.

(Distribution Limitation Statement A)

CONTENTS

Preceding page blank

ILLUSTRATIONS

TABLES

SECTION I

INTRODUCTION

During the Lunar missions, the radiation environment of the astronauts is quite complex. The radiation consists primarily of protons and ^{4}He nuclei with less than 2 percent of the particles being high Z, heavy nuclei. The heavy, high Z nuclei consist primarily of nuclei of carbon (Z=6) through iron (Z=26). However, recently the presence of small fluxes of super heavy nuclei such as lead (Z=82) and uranium (Z=92) has been experimentally established. The intensity and the energy spectra of these particles varies with time and position within the spacecraft. The long term time variations come about due to the changes in the 11 year solar cycle, the rapid short term variations are due to solar emissions, such as the solar flares. The radiation environment inside the spacecraft is also significantly influenced by the shielding offered by the various components of the spacecraft and indeed, by the bodies of the astronauts themselves. Since the Apollo shielding varies from about 2 to 260 g/cm^2 depending on the direction, the incoming radiation is highly aniso-tropic.

Background low LET (linear energy transfer) radiation is a part of everyday life, however the high LET radiation produced by the high Z particles is unique to the space environment. While the radiobiological action of this radiation is poorly understood, particularly when it comes to the possible long term, delayed effects, certain definite effects on biological systems have been observed. For example it has been demonstrated that high LET radiation is particularly effective in cell inactivation of certain non-regenerative cells [human kidney (T1) cells, for example]. A more dramatic effect of multicharged

1

particles has been the light-flash phenomenon observed by the Apollo astronauts.
It becomes important then to measure the exposure of individuals to these
radiations so that this information will be available as part of the medical
histroy and subject to future interpretations.

The technique for the measurement of dose due to protons is well under-
stood; however, the dosimetry of heavy ions is much more complicated. Indeed
in this case the whole concept of dose is not very meaningful. The energy
associated with heavy ions is concentrated within a limited volume of tissue,
so that direct effects along the particle track are far more pronounced than
for lighter particles even when the absorbed dose, measured macroscopically,
is the same. A knowledge of how such particle tracks are distributed within a
given biological volume now becomes a significant dosimetric parameter.

In Table I is given the relevant data on Apollo missions 8-14. This
includes the mission type, launch date, duration, as well as the astronaut and
detector packet designation.

Table I

MISSION DATA AND PACKET DESIGNATION

CM, Command module; LM, Lunar module; LS, Lunar surface

Apollo Mission	Mission Type	Date and Duration	Astronaut	Location On Astronaut	Location	Packet Designation
8	Lunar Orbiting	12/21/68 147 hours	W. M. Anders	ankle	CM	3C
10	Lunar Orbiting	5/18/69 192 hours	E. Cernan	ankle	CM, LM	C1
			J. W. Young	ankle	CM	B6
			J. W. Young	chest	CM	A2
11	Lunar Landing	7/16/69 195 hours	M. Collins	ankle	CM	2C
			N. A. Armstrong	ankle	CM, LM, LS	1C
			N. A. Armstrong	chest	CM, LM, LS	1A
12	Lunar Landing	11/14/69 244.5 hours	R. F. Gordon	ankle	CM	2C
			C. Conrad	ankle	CM, LM, LS	3C
			C. Conrad	chest	CM, LM, LS	3A
13	Lunar Flyby	4/11/70 143 hours	F. W. Haise	ankle	CM	3C
			J. L. Swigert	ankle	CM	2C
			J. L. Swigert	chest	CM	2A
14	Lunar Landing	1/31/71 216 hours	E. D. Mitchell	ankle	CM, LM, LS	3C
			S. A. Roosa	ankle	CM	1C
			E. D. Mitchell	chest	CM, LM, LS	3A

3

SECTION II

METHODS AND PROCEDURES

On Apollo missions, the individual astronauts' high Z particle exposure was measured by means of Lexan foils. The foils are located in the passive dosimetry packs carried on the chest, thigh, and ankle of each astronaut. On Apollo missions 8-12 each plastic packet consisted of two, 190 micron thick layers of type 8070-112 Lexan. On Apollo 13 and subsequent missions three layers were used. The addition of the third layer was found to significantly improve the charge resolution of the detector stack. Each detector has an area of about 8 cm². The layers are held stationary with respect to each other by means of a heat seal on each edge. In order to reduce the number of variables, all Lexan foils flown to date have been taken from the same batch of Lexan.

Detector Processing

After each flight, the Lexan foils are given large exposures of ultraviolet radiation for sensitization (Ref. 1) and then processed in NaOH solution to etch the conical particle tracks. Tracks are located by scanning with an optical microscope usually at 200 X magnification. Each detector is scanned independently by at least two different observers. For Z determination, measurements are performed at 600 X in each of the surfaces where a visible etch cone is found (Ref. 2). Particle identification is accomplished either by measuring the particles' LET at a given residual range (for particles stopping in the detector), or by measuring the LET and its rate of change with the residual range (Ref.3). It is usually possible to determine the particles charge, energy and its direction of travel.

In order to eliminate the possibility of differences in detector sensi-

4

tivity arising from the differences in processing of one batch of detectors to the next, the different detectors listed in Table I were processed in four series. Series I included detectors: A8-3C, A10-C1, A11-2C, A12-2C, and A13-2C. Series II included detectors: A10-B6, A11-1C, A12-3C, and A13-2C. Series III included detectors: A10-A2, A11-1A, A12-3A and A13-2A. Series IV included all detectors of Apollo 14. All detectors flown to date were assembled from a single batch of Lexan, and in a single processing-calibration cycle were included detectors from five different Apollo missions. This procedure enhances considerably the confidence in any intercomparison of measurements for the different missions.

Detector Calibration

For each particle which does not stop in the Lexan packet (the typical situation) the information available about this particle is the track etch rate as a function of position along the trajectory. Calibrating the detector packet consists of relating the etch rate to some function of particle atomic number, Z, atomic weight, A, and residual range, R. Here, rather than the energy, the residual range is used as an independent variable because it is more closely related to the measurement situation. Theoretical reasoning indicates that the sought function is approximated by the particle linear energy transfer, LET_ω*. It is found that LET_{350} represents the experimental situation well.

Over the range of Z and R applicable to our measurements LET_{350} can be represented as a power function in Z, A, and R. Since isotopic separation is not feasible in such thin packets, the approximate relationship between Z and A for the most abundant isotope of an element,

---

* LET_ω is the energy transfer per path length to electrons receiving less than ω electron volts of energy per electron.

$$A = 1.78\ Z^{1.052}, \tag{1}$$

is used. Then LET_{350} is given by

$$LET_{350} = 0.1249\ Z^{1.553}\ R^{-0.472}\ \text{MeV}/\mu, \tag{2}$$

where R is in microns.

Experimentally it is found that the track etch rate, V_T, can also be represented as a power function of LET_{350} for values of $V_T \lessapprox 100\ \mu/\text{hour}$.

$$V_T = 82.0\ C_R\ LET_{350}^{2.12} \tag{3}$$

The value of the exponent of LET_{350}, 2.12, is very nearly the average value found from numerous calibration runs. Its precise value is chosen to be consistent with a reciprocal relationship between the particle residual range and the track etch rate.

The value of C_R is determined experimentally using 10MeV/nucleon ^{16}O and ^{20}Ne particles accelerated by the Berkeley Hilac (heavy ion linear accelerator). Their etch rate is measured by etching the UV irradiated samples and measuring the track length. Since the incident energy of the particles and their residual range at the entrance surface of the plastic is known, the energy and LET can also be determined at any point along the trajectory. To obtain the values of V_T in Equation (3) the measured etch rates are first corrected to compensate for the variation of the track sensitization with depth in the detector. This variation is caused by the attenuation of the sensitizing UV. The correction is accomplished using the semi-empirical result that the real track etch rate varies approximately as the depth in sample to the -0.1 power. With this approximation the value of V_T 1μ below the detector surface is computed from the measured average etch rate. Table II summarizes the calibration data. The track etch rate as corrected for UV attenuation is given in Column 6. The average residual range, energy per nucleon, and LET values are the values at the track center. For each UV series two oxygen measurements are indicated. These were

6

Table II

Detector Calibration Data

Series	Ion	Track length (μ)	Etch time (hours)	Etch rate $\left(\frac{\mu}{\text{hour}}\right)$	Corrected etch rate $\left(\frac{\mu}{\text{hour}}\right)$	Ave. residual range (μ)	Energy/ nucleon $\left(\frac{\text{MeV}}{\text{nuc}}\right)$	LET_{350} $\left(\frac{\text{MeV}}{\mu}\right)$	C_R $\left(\frac{\mu^2}{\text{hour}}\right)$
1	O	6.5	0.772	8.4	8.9	299.3	10.2	0.212	
	Ne	16.0	0.503	31.8	34.3	251.0	10.2	0.331	2.815
	O	41.8	0.772	54.1	69.1	56.1	3.5	0.496	
2	O	22.3	3.000	7.4	8.9	291.4	10.0	0.215	
	Ne	71.5	3.000	23.8	29.8	223.2	9.5	0.349	2.863
	O	77.4	3.000	25.8	34.7	71.2	4.1	0.441	
3	O	23.3	3.367	6.8	8.2	291.0	10.0	3.215	
	Ne	62.9	3.193	19.7	26.2	227.6	9.6	0.346	2.744
	O	69.6	3.367	20.7	27.2	67.9	4.0	0.451	
4	O	27.6	3.920	7.0	8.6	288.7	10.0	0.216	
	Ne	76.4	3.957	19.3	26.2	220.8	9.4	0.351	2.851
	O	91.5	3.920	23.4	32.2	78.8	4.4	0.424	

7

measured on opposite surfaces of the same Lexan sheet for the 45° dip angle particles, which passed all the way through the layer. These 1μ depth values of V_T are then plotted on a log-log plot against the value of LET_{350} at the track center. Fitting a slope of 2.12 line then gives C_R, which is given in Table II for each UV series. All measured track etch rates in the dosimetry packets are corrected for UV attenuation in the same way. Thus calibration is not dip angle or etch time dependent and can be applied to all tracks in these packets.

The basic relationship used in reducing data of the Lexan packets is obtained by combining equations (2) and (3).

$$R = \frac{C_R \, Z^{3.29}}{V_T} \qquad V_G < V_T \lesssim 100 \ \mu/\text{hour.} \tag{4}$$

The parameter V_G is the bulk etch rate of the UV irradiated Lexan. Four different UV irradiations were used for the plastic detectors covered by this report. The values of C_R vary from 2.744 through 2.863 μ^2/hour, the average value being $2.818 \pm 0.027 \ \mu^2/\text{hour}$. The values of V_G vary from 2.11 through 3.06 μ/hour, the average being 2.49 ± 0.18.

Track Registration Criterion

The absolute requirement for track registration is that the vertical component of the track etch, $V_T \sin \delta$, be greater than V_G. Here δ is the dip angle of the trajectory. If V_T satisfies this requirement at the point where the trajectory intersects an etching surface, a track will be formed. If this condition is only marginally met, however, the track will be quite small and may escape detection even in the most meticulous scanning process. If V_T from the registration criterion is substituted into equation (4), it can be seen that for absolute registration,

$$R < R_{reg} = C_R \frac{Z^{3.29} \sin \delta}{V_G} \, , \tag{5}$$

where R_{reg} is the particle registration range (Ref. 3).

Since in practice the smallest tracks are usually missed by nearly all scanners, an efficiency, ε is introduced. If it is assumed that all values of R are equally probable, the effective, realistic registration criterion is given by

$$R < \varepsilon R_{reg} \tag{6}$$

Here it is not assumed that the scanning efficiency is 100% for $R < \varepsilon R_{reg}$ and 0% for $R > \varepsilon R_{reg}$. Rather, ε is defined such that as many particle tracks are lost due to scanning inefficiency for tracks with $R < \varepsilon R_{reg}$ as are found for those with $R > \varepsilon R_{reg}$. Furthermore, it has been experimentally demonstrated that ε need not be considered a function of δ and theoretically demonstrated that it is not a function of Z.

Particle Charge Measurement

Equation (4) shows that R is a linear function of V_T^{-1}, the coefficient being $C_R Z^{3.29}$. To obtain Z, the distance along the trajectory from any convenient reference point is plotted as a function of the reciprocal of the measured track etch rate. The slope of the best fit straight line through these points, $\frac{dR}{dV_T^{-1}}$ is then used to compute Z from the equation,

$$Z = \left(\frac{1}{C_R} \frac{dR}{dV_T^{-1}} \right)^{0.304} \tag{7}$$

Of course, if the particle actually stops in the packet, the value of R can be measured directly, and Z can be obtained using equation (4). An example of a Z determination plot is given in Figure 1.
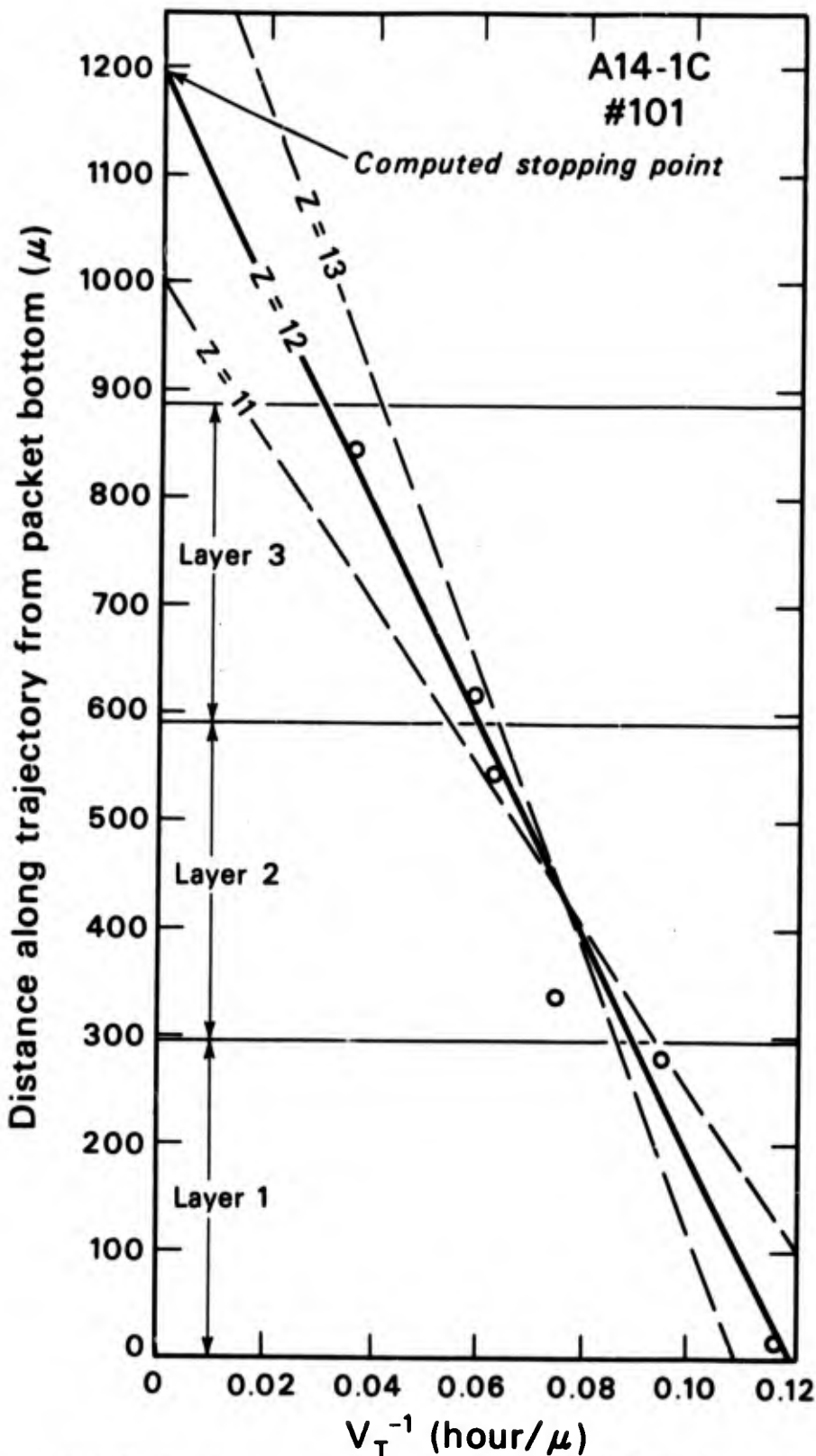
Figure 1. Z determination plot. The six points are the measured points from a Mg ion which leaves the astronaut, traverses the plastic, and stops outside the plastic. It enters the plastic with an energy of 27.9 MeV/nucleon and leaves with an energy of 12.6 MeV/nucleon (a residual range of 310 μ or 36.5 mg/cm² in Lexan). The charge resolution capability is shown by the dashed lines for Z=11 and 13.

Particle Fluences

The fluence of the primary particles (tracks/cm^2) is given in Table III for one detector packet of Apollo 8 and three detector packets from each of the subsequent flights except Apollo 9. Apollo 9 is not included because no primary cosmic ray particles were observed in the Lexan detectors due to the high rigidity cosmic ray spectrum in this type of near-equatorial earth orbit (for a similar exposure see reference 4). In the column labeled "Location" CM signifies the command module, LM the lunar module, and LS the lunar surface. The "observed" track fluence is the total fluence of all tracks found by all scanners. The "corrected" fluence is the fluence of all tracks which register in the detector, i.e. all tracks with the vertical component of the track etch rate greater than the bulk etch rate of the detector.

To determine the number of particles which register in the packet, i.e. the number of tracks actually found divided by ε, the integral distribution in track size for large tracks is extrapolated to zero track size. This process assumes that for large tracks the scanning efficiency is nearly 100%. This assumption is supported in two ways: 1) For large tracks all scanners find the same and only the same tracks. 2) The distribution in track size follows the theoretically predicted distribution curve shape for large tracks and can be seen to fall off from this distribution rather rapidly at a specific, small track size if the correct parameter is used in measuring a track size.

The experimentally confirmed parameter which governs the scanner's ability to see a track is $V_T \sin \delta / V_G$. In most cases, rather than measuring both track

11

Table III

High Z Cosmic-Ray Track Fluences From Apollo Passive Dosimeters

Apollo Mission	Packet Designation	Observed Track Fluence (No./cm²)	Corrected Track Fluence (No./cm²)	Track Fluence (LET$_{350}$>0.15MeV/u) (No./cm²)	Flight Ave. Track Fluence (LET$_{350}$>0.15MeV/u) (No./cm²)	Flight Ave. Track Flux (LET$_{350}$>0.15MeV/u) (No./cm² day)
8	3C	2.64	3.06	2.44 ± 0.49	2.44 ± 0.49	0.398 ± 0.080
10	C1	4.06	5.85	4.66 ± 0.66		
	B6	3.41	6.09	4.58 ± 0.71	4.20 ± 0.36	0.525 ± 0.045
	A2	2.80	2.97	3.27 ± 0.58		
11	2C	3.54	5.04	4.01 ± 0.76		
	1C	3.52	4.64	3.65 ± 0.69	4.35 ± 0.47	0.535 ± 0.058
	1A	4.08	5.16	5.76 ± 1.02		
12	2C	6.07	8.02	6.38 ± 1.00		
	3C	4.87	5.79	4.77 ± 0.77	5.49 ± 0.53	0.539 ± 0.052
	3A	3.99	4.96	5.46 ± 1.02		
13	3C	6.13	7.70	6.13 ± 0.91		
	2C	4.08	5.23	4.10 ± 0.75	5.11 ± 0.50	0.858 ± 0.084
	2A	4.05	4.86	5.10 ± 0.93		
14	3C	6.38	8.49	8.07 ± 1.14		
	1C	8.61	10.64	10.23 ± 1.24	7.35 ± 0.30	0.817 ± 0.033
	3A	6.33	7.44	6.91 ± 0.98		

length and dip angle for the tracks found through scanning, only the semi-minor axis of the elliptical track openings, b, is measured (Ref. 2), and the geometrical relationship,

$$\frac{V_T \sin \delta}{V_G} = \frac{1 + \left(\frac{b}{B}\right)^2}{1 - \left(\frac{b}{B}\right)^2},$$ (8)

is used to determine $V_T \sin \delta / V_G$. Here B is the amount of bulk material removed from the detector surface.

The specific details of the correction are as follows. Dividing Equation (4) by Equation (5) gives

$$\frac{R}{R_{reg}} = \frac{V_G}{V_T \sin \delta} = \frac{1 - \left(\frac{b}{B}\right)^2}{1 + \left(\frac{b}{B}\right)^2}$$ (9)

With the assumption that all values of R are equally probable, the integral distribution in b, $N_{b>b_0}$, follows.

$$N_{b>b_0} = N_{b>0} \left[\frac{1 + \left(\frac{b_0}{B}\right)^2}{1 - \left(\frac{b_0}{B}\right)^2}\right]^{-1}$$ (10)

where $N_{b>0}$ is the total number of tracks which register in the packet. Also, if N is the number of tracks found,

$$\epsilon = \frac{N}{N_{b>0}}.$$ (11)

To determine $N_{b>0}$, $N_{b>b_0}$ is plotted on a log-log plot against $\dfrac{1 + \left(\frac{b_0}{B}\right)^2}{1 - \left(\frac{b_0}{B}\right)^2}$ and a slope -1 is drawn through the portion of the curve which does not show loss of tracks due to scanning inefficiency. This line is then extrapolated to $b_0 = 0$ to obtain $N_{b>0}$. Figure 2 illustrates an integral b distribution and the correction procedure.
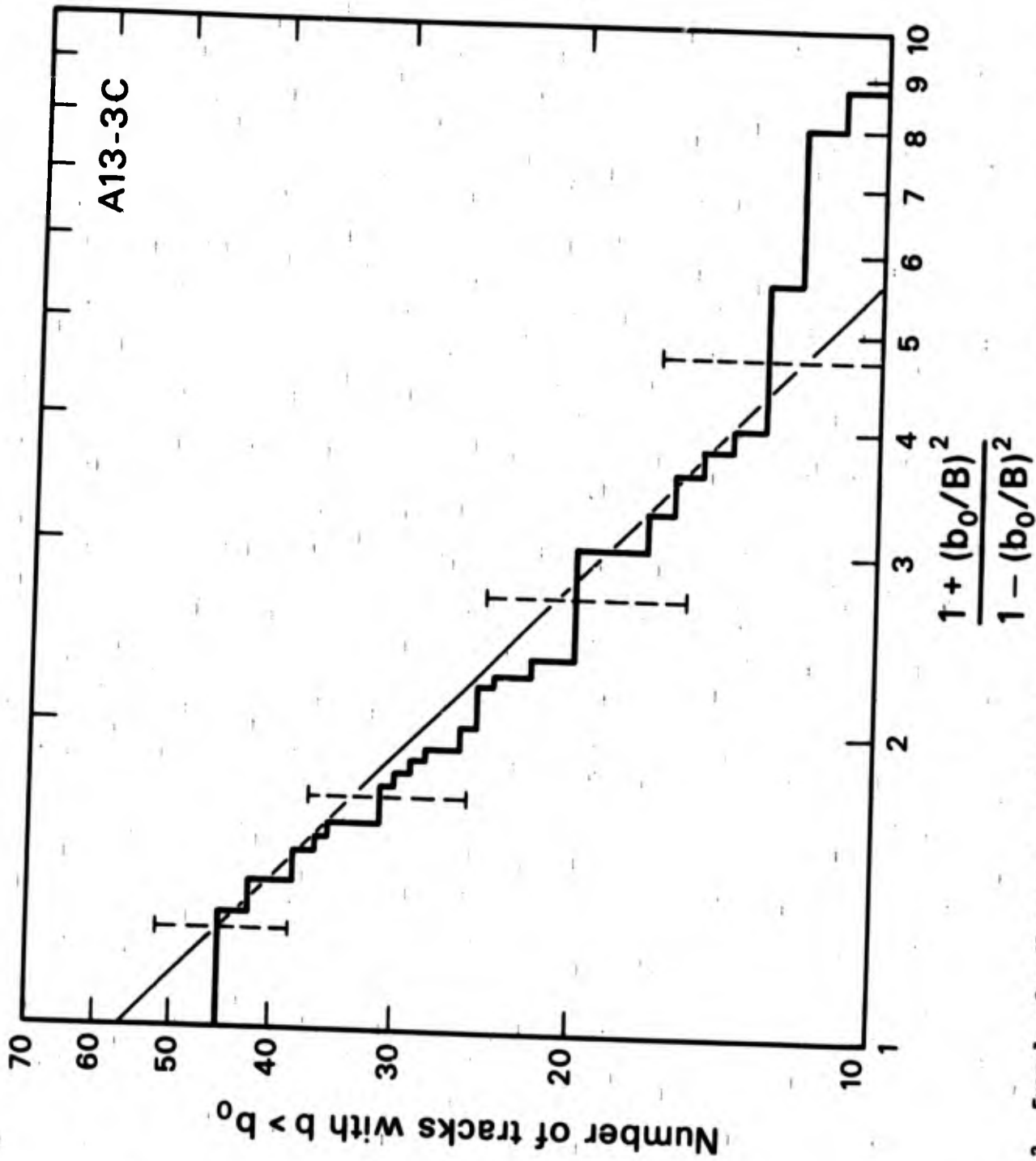
Figure 2. Example of a fluence correction plot. The slope -1 curve drawn through the experimental distribution shows the expected number of registerable tracks to be 56 although only 45 of them were found through scanning.

14

The track fluence of particles with $LET_{350} > 0.15$ MeV/µ (see Table III) is obtained from the integral LET spectra to be described later. It differs from the "corrected" fluence in having taken the detector sensitivity as well as the scanning efficiency into account. It is an absolute measure of the cosmic ray beam fluence and therefore can be used for comparison of different detector locations and different flights. Since the sensitivity varies slightly from detector to detector, the typical LET cutoff value of 0.15 MeV/µ was arbitrarily chosen as a fixed, absolute cutoff value.

The flight average of the LET > 0.15 MeV/µ particle fluence (see Table III) is the total number of tracks with LET > 0.15 MeV/µ divided by the total area of the packets used in obtaining the average. The average values given in Table III were obtained as follows: for Apollo 8 only one packet was used, for each of the Apollo flights 10-13 the three listed packets were included, and for Apollo 14 all ten packets were included in obtaining the average values given (Ref. 5).

The increase in the measured high Z particle fluence observed in the recent missions is only partially accounted for by the longer duration of the latter missions. The decrease in the degree of solar modulation also plays a role in contributing to higher recorded cosmic ray fluences. This is shown under "Flight Ave. Track Flux" in Table III. Here the flight average $LET_{350} > 0.15$ MeV/µ track fluence was divided by the total flight time in days to obtain the flux. Although these flux values do not take into account the variation of the shielding during each mission, the increase in the flux from Apollo 8 through Apollo 14 is still quite significant.

Ender Density

To reduce the measured distribution of track parameters into a more meaningful and less detector dependent form two assumptions are made:

1) The time average of the particle beam over each detector hemisphere is isotropic.

2) All particle residual ranges are equally probable.

Assumption 1) is based on the motion of the crew members. Although each of their radiation environments is highly anisotropic, they are frequently changing position and orientation. Thus the only remaining anisotropy after this averaging process is provided by the shielding of the astronauts. Since the detectors are placed flatly against the astronaut, this anisotropy is basically from one hemisphere to the other, which is allowed in the assumption.

Assumption 2) is based on the relatively short registration ranges of the particles [Equation (5)]. This means that the particles seen in the packet all stop very close to it. Thus, the registered particles come from a very narrow portion of the external (to the spacecraft) cosmic ray energy spectrum, over which there is only a small variation in particle flux.

From the two assumptions listed above it is possible to write the distribution of the spherical (falling on a sphere of unit area) particle fluence in residual range and solid angle as,

$$\frac{d^3 N_Z}{dA_p \, dR \, d\Omega} = \frac{\rho_Z}{4\pi} , \tag{12}$$

where N_Z is the number of particles of atomic number Z, dA_p is the element of projected (normal to the beam) area, $d\Omega$ is the element of solid angle, and ρ_Z is the ender density or number of stopping particles of atomic number Z per volume. If it is realized that the sense of the particle travel does not affect its registration appreciably, the dip angle, δ, can be considered to lie in the range 0 through $\pi/2$ radians. Then $dA_p = dA \sin \delta$ and $d\Omega = 4\pi \cos \delta \, d\delta$ (both senses of travel included). Equation (12) becomes

$$\frac{d^3 N_Z}{dA \, dR \, d\delta} = \rho_Z \cos \delta \sin \delta \tag{13}$$

16

Since by the above assumptions ρ_z is neither a function of R nor δ, Equation (13) can be integrated over the range of R for which registration occurs to obtain the distribution of the measured particle fluence in δ,

$$\frac{d^2N_z}{dA\,d\delta} = \rho_z \cos\delta\sin\delta \int_0^{\epsilon R_{reg}} dR = \frac{\epsilon\,C_R\,Z^{3.29}\,\rho_z}{V_G} \cos\delta\sin^2\delta \qquad (14)$$

Agreement between Equation (14) and experimental dip angle distributions confirms that ϵ is not dip angle dependent.

Integrating again over the possible range of δ gives the measured particle fluence,

$$\frac{dN_z}{dA} = \frac{\epsilon\,C_R\,Z^{3.29}\,\rho_z}{V_G} \int_0^{\pi/2} \cos\delta\sin^2\delta\,d\delta = \frac{\epsilon\,C_R\,Z^{3.29}\,\rho_z}{3V_g} \qquad (15)$$

Equation (15) shows that the measured fluence depends on the scanning efficiency, ϵ, the etch rate calibration, C_R, the bulk etch rate V_G, and very strongly on the particle atomic number Z. The total measured fluence for all types of particles is given by,

$$\frac{dN}{dA} = \sum_Z \frac{dN_z}{dA} = \frac{\epsilon C_R}{3V_G} \sum_Z Z^{3.29}\,\rho_z \qquad (16)$$

and the ender density by

$$\rho_z = \frac{3V_G}{C_R\,Z^{3.29}} \frac{1}{\epsilon} \frac{dN_z}{dA} \qquad (17)$$

The integral distribution in ender density which is given for three of the Apollo packets in Figures 2, 3, and 4, is given by

$$\rho_{z\geq z_0} = \frac{3V_G}{C_R\epsilon} \sum_{z_0}^{\infty} Z^{-3.29} \frac{dN_z}{dA} \qquad (18)$$

Because of the uncertainty of the Z determination in the thin packets and because of the known preponderance of even Z values in the cosmic ray spectrum, all measured values of Z were adjusted to the most probable even Z value for

17

these integral distributions. Also, to maintain the proper fluence, the few particles whose Z values could only be specified as a lower bound were appropriately distributed over the larger Z values according to the distribution already established by those particles with measurable Z values. Three Z spectra are given in Figures 3 to 5 to illustrate the ender densities of particles which register in statistically significant numbers and provide a basis for the slightly Z spectrum dependent conversion from the measured LET_{350} spectrum to the LET_∞ spectrum necessary for fractional cell loss computations.

Integral LET Spectrum

From the calibration and the corrected fluence, $\frac{1}{\epsilon}\frac{dN}{dA}$, it is possible to obtain a theoretical LET spectrum, i.e. one for which individual values of V_T [and thus LET_{350} through Equation (3)] have not been measured. Using Equation (2) and its derivative, Equation (12) becomes

$$\frac{d^3N_Z}{dA_p \, d\Omega \, dLET_{350}} = 0.00206 \, Z^{3.29} \, \rho_Z \, LET_{350}^{-3.12} .\tag{19}$$

Then summing over Z and using Equation (16) gives the differential LET_{350} spectrum,

$$\frac{d^3N}{dA_p \, d\Omega \, dLET_{350}} = \frac{0.0617 \, V_G}{C_R} \frac{1}{\epsilon}\frac{dN}{dA} \, LET_{350}^{-3.12} .\tag{20}$$

Integrating gives the integral LET_{350} spectrum,

$$\frac{d^2N(LET_{350}>L)}{dA_p \, d\Omega} = \frac{0.00291 \, V_G}{C_R} \frac{1}{\epsilon}\frac{dN}{dA} \, L^{-2.12} = C_L \, L^{-2.12} .\tag{21}$$

The measured values of C_L for individual packets and the flight average values of C_L are given in Table IV. These values of C_L are for L in MeV/μ. The flight average for Apollo 14 is for ten packets, not just three (Ref. 5). All of the listed uncertainties are those due to counting statistics.

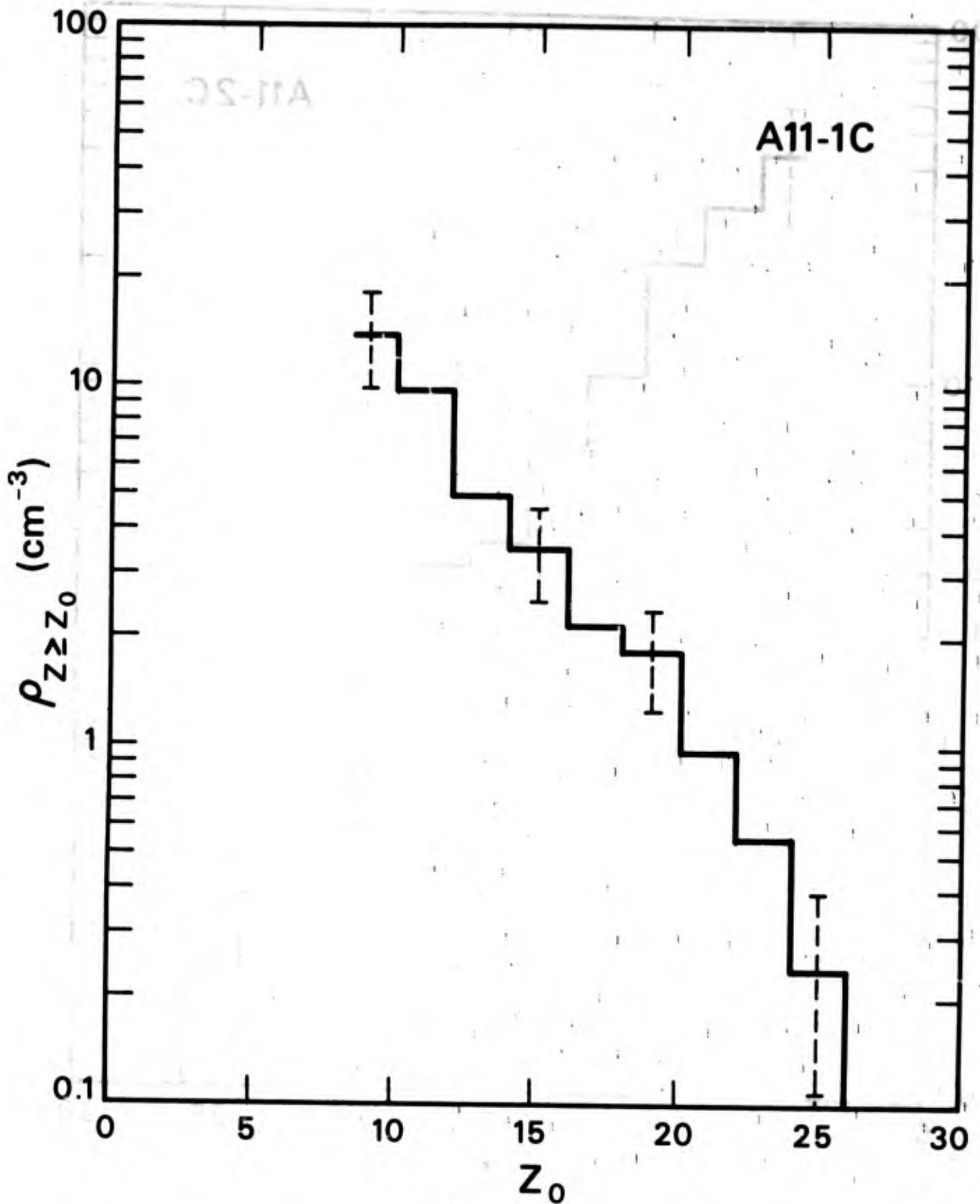At this point it is appropriate to discuss the track fluence of particles

18

Figure 3. Ender density as an integral Z spectrum for Apollo 11 - 1C. The number of stopping particles/cm² with Z ≥ Z_0 is given. The error bars indicate the errors due to counting statistics.
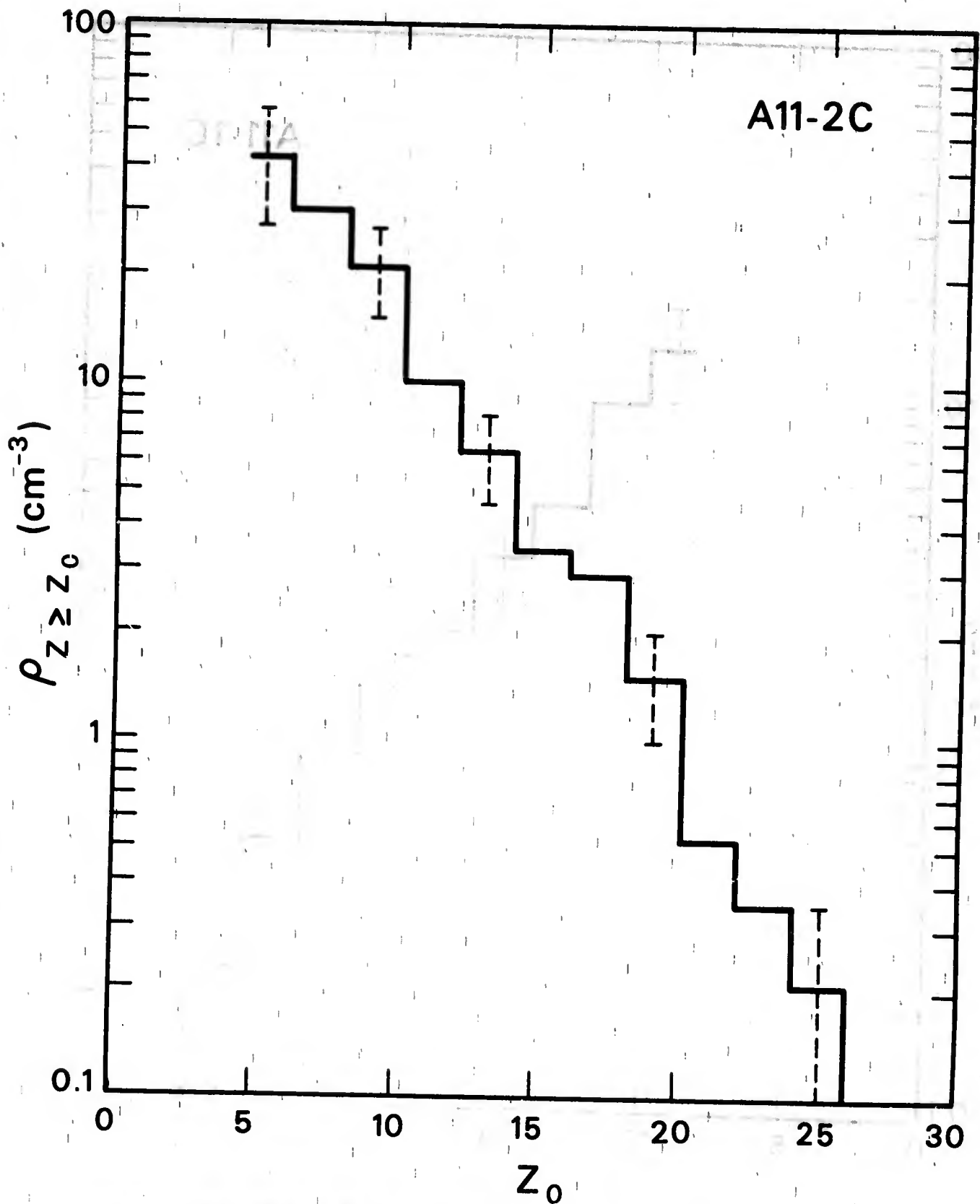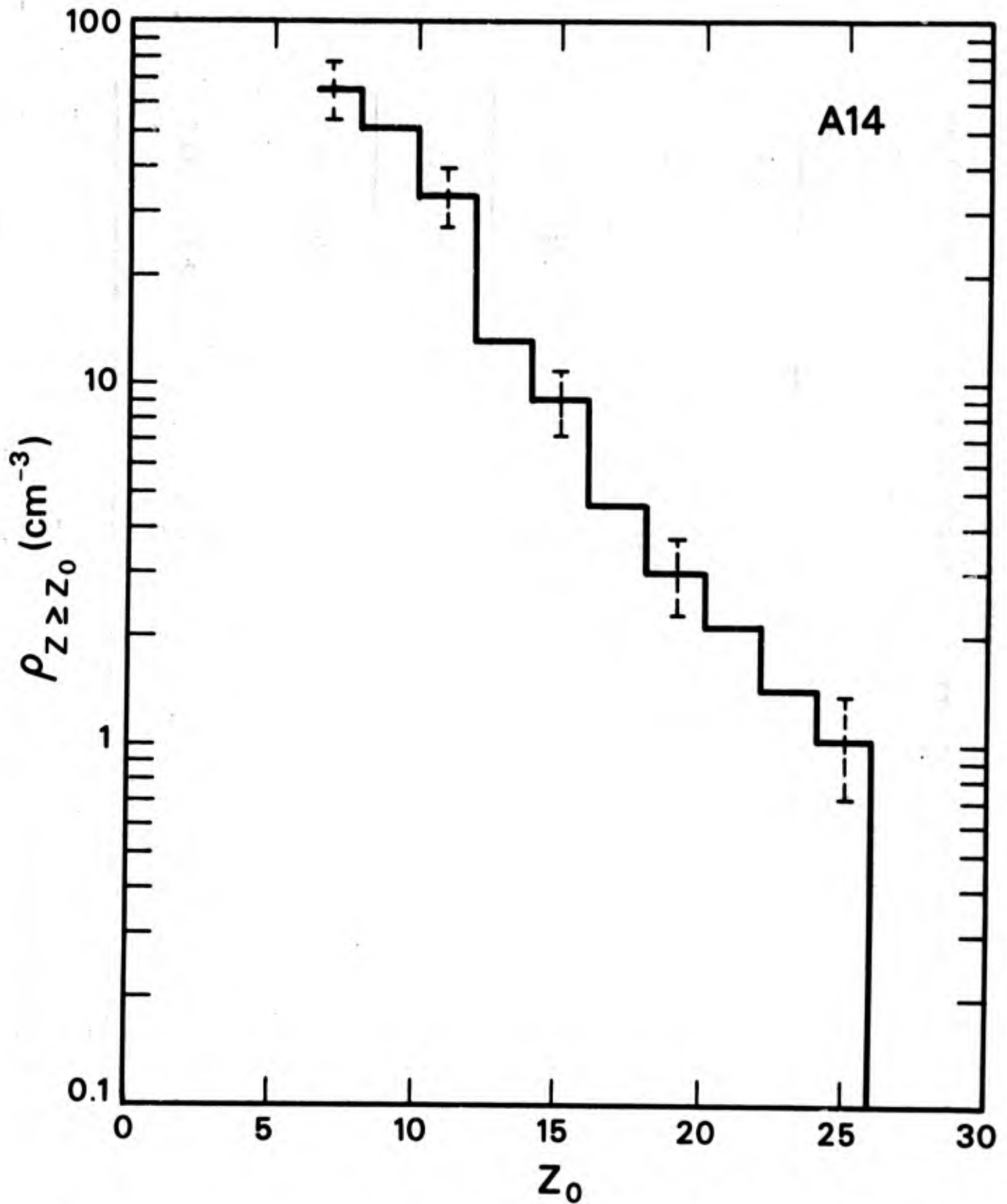
Figure 4. Ender density as an integral Z spectrum for Apollo 11 - 2C. The number of stopping particles/cm² with $Z \geq Z_0$ is given. The error bars indicate the errors due to counting statistics.

Figure 5. Ender density as an integral Z spectrum for Apollo 14. The number of stopping particles/cm^2 with $Z \geq Z_0$ is given. The error bars indicate the errors due to counting statistics.

Table IV

Measured Coefficients of the Integral LET_{350} Spectrum, C_L, and Flight Average Values.

Apollo Mission	Packet Designation	Coefficient of integral LET spectrum, C_L (10^{-2} part./cm²ster)	Flight Ave. of C_L (10^{-2} part./cm²ster)
8	3C	0.70	0.70 ± 0.14
10	C1 B6 A2	1.33 1.31 0.93	1.20 ± 0.10
11	2C 1C 1A	1.15 1.04 1.64	1.24 ± 0.13
12	2C 3C 3A	1.82 1.36 1.56	1.57 ± 0.15
13	3C 2C 2A	1.75 1.17 1.46	1.46 ± 0.14
14	3C 1C 3A	2.31 2.92 1.98	2.19 ± 0.10

with $LET_{350} > 0.15$ MeV/μ given earlier. The $LET_{350} > 0.15$ MeV/μ fluence, $\frac{dN (LET_{350} > 0.15 \text{ MeV/μ})}{dA}$, is obtained directly from Equation (21) by using $L = 0.15$ and multiplying by an effective solid angle of 2π. A solid angle of 4π is not used because the average projection factor is $\frac{1}{2}$. This gives

$$\frac{dN (LET_{350} > 0.15 \text{ MeV/μ})}{dA} = \frac{1.02 \ V_G}{C_R} \frac{1}{\epsilon} \frac{dN}{dA} \qquad (22)$$

The LET_{350} spectrum can also be computed directly from the measured values of the track etch rate. The values of LET_{350} are computed using Equation (3). For particles intersecting the detector surface with $LET_{350} >> LET_c$, the cutoff value of LET_{350}, almost all of the tracks register and are found during the scanning process, giving an effective solid angle of 2π. As LET_{350} decreases, some tracks are lost at low dip angles. The effective cutoff dip angle, δ_c, can be obtained from Equations (3), (6), and (9). It is given by

$$\sin \delta_c = \left(\frac{LET_c}{LET_{350}} \right)^{2.12} \qquad (23)$$

where $LET_c = 0.125 \left(\frac{V_G}{\epsilon C_R} \right)^{0.472}$. With an isotropic differential LET_{350} spectrum, $\frac{d^3N}{dA_p \ d\Omega \ dLET_{350}}$, the measured differential spectrum, $\frac{d^2N}{dA \ dLET_{350}}$, is given by integrating the element of solid angle times the projection factor over the available values of δ.

$$\frac{d^2N}{dA \ dLET_{350}} = 4\pi \frac{d^3N}{dA_p \ d\Omega \ dLET_{350}} \int_{\delta_c}^{\frac{\pi}{2}} \cos \delta \sin \delta \ d\delta = 2\pi \left(1 - \left(\frac{LET_c}{LET_{350}} \right)^{4.14} \right) \frac{d^3N}{dA_p \ d\Omega \ dLET_{350}}$$

or

$$\frac{d^3N}{dA_p \ d\Omega \ dLET_{350}} = \frac{1}{2\pi} \left(1 - \left(\frac{LET_c}{LET_{350}} \right)^{4.14} \right)^{-1} \frac{d^2N}{dA \ dLET_{350}} \qquad (24)$$

Then the measured integral LET_{350} spectrum is obtained by summing rather than integrating over all values of $LET_{350} \geq L$

$$\frac{d^2N \; (LET_{350} \geq L)}{dA_p \; d\Omega} = \frac{1}{2\pi A} \sum_{LET_{350,i} \geq L} \left[1 - \left(\frac{LET_C}{LET_{350,i}} \right)^{4.14} \right]^{-1} \tag{25}$$

where A is the packet area and $LET_{350,i}$ is the value of LET_{350} for the ith particle.

One measured integral LET_{350} spectrum for each of the Apollo flights is given in Figures 6 through 11. The corresponding theoretical integral LET_{350} spectra are shown as straight diagonal lines. It can be seen that the measured spectra are well approximated by the theoretical spectra.

Fractional Cell Loss

Typically, radiation exposures are measured in terms of a dose or dose equivalent for high LET particles. For very high LET particles a more meaningful measure of the effect of radiation is the fractional cell loss, FCL. Although FCL has been difficult to measure for human cells because of the unavailability of appropriate particle accelerators, Todd (Ref. 6) has succeeded in measuring the cross section for irreversible inactivation, σ_1, for human kidney (T1) cells in vitro. For the applicable range of LET his results can be represented by

$$\sigma_1 = \begin{cases} 12.9 \, LET_\infty^{1.51} \, , & 0.1 < LET_\infty < 3.6 \text{ MeV cm}^2/\text{mg} \\ 90 \, , & LET_\infty \geq 3.6 \text{ MeV cm}^2/\text{mg} \end{cases} \tag{26}$$

Here, σ_1 is expressed in μ^2. With the approximate relation

$$LET_\infty = 1.19 \; Z^{1.59} \; R^{-0.437}, \tag{27}$$

where R is in μ and LET_∞ in MeV cm²/mg, and the average of the three measured Z spectra, it can be shown that

$$\frac{d^3N}{dA_p \; d\Omega \; dLET_\infty} = 715 \; C_L \; LET_\infty^{-3.29} \tag{28}$$

It should be noted that the units of LET_ω as well as the value of ω have been changed to match those of Todd's measurements. The FCL due to particles with
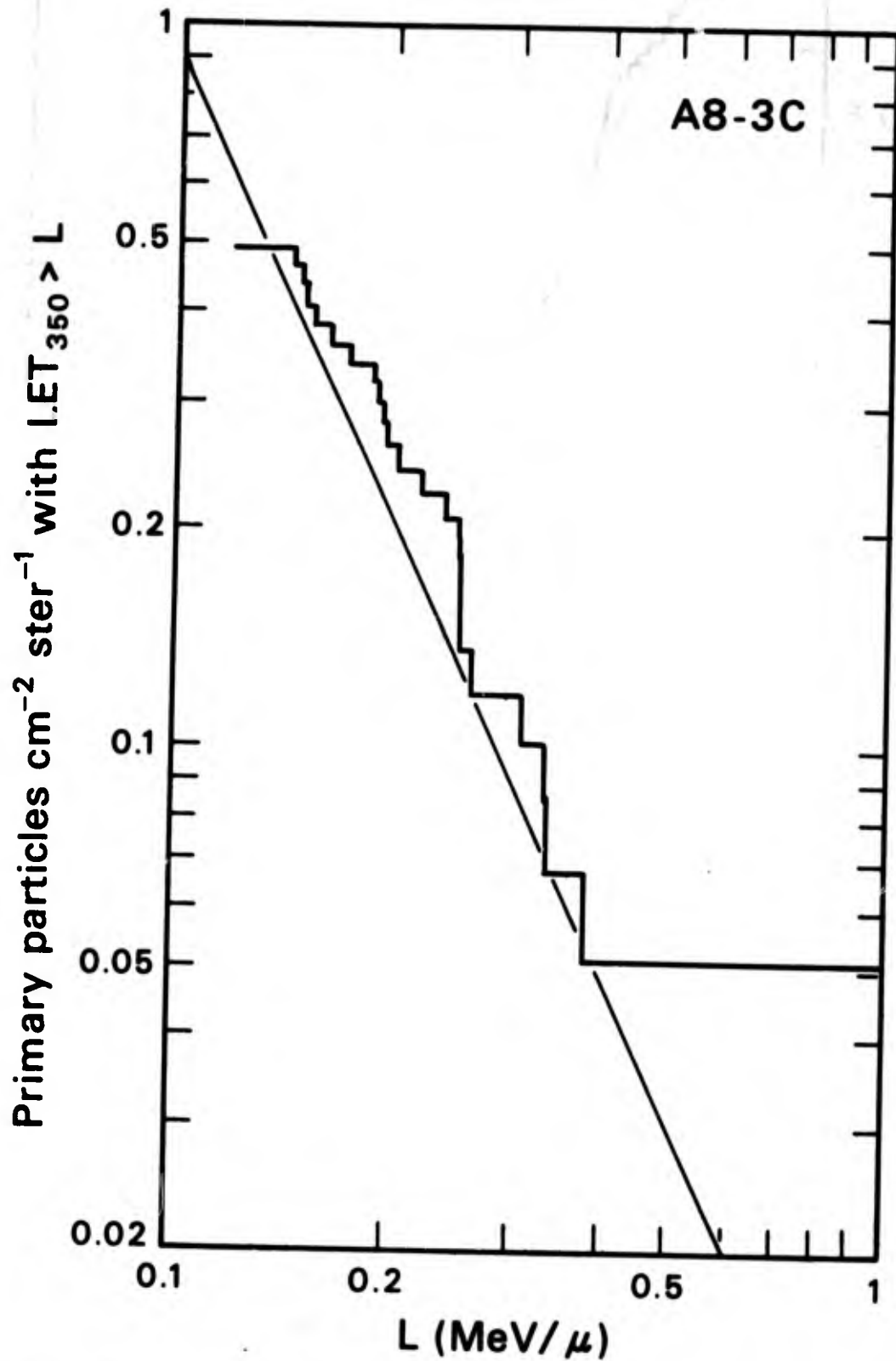
24

Figure 6.   Measured integral LET$_{350}$ spectrum from Apollo 8 - 3C.   For comparison
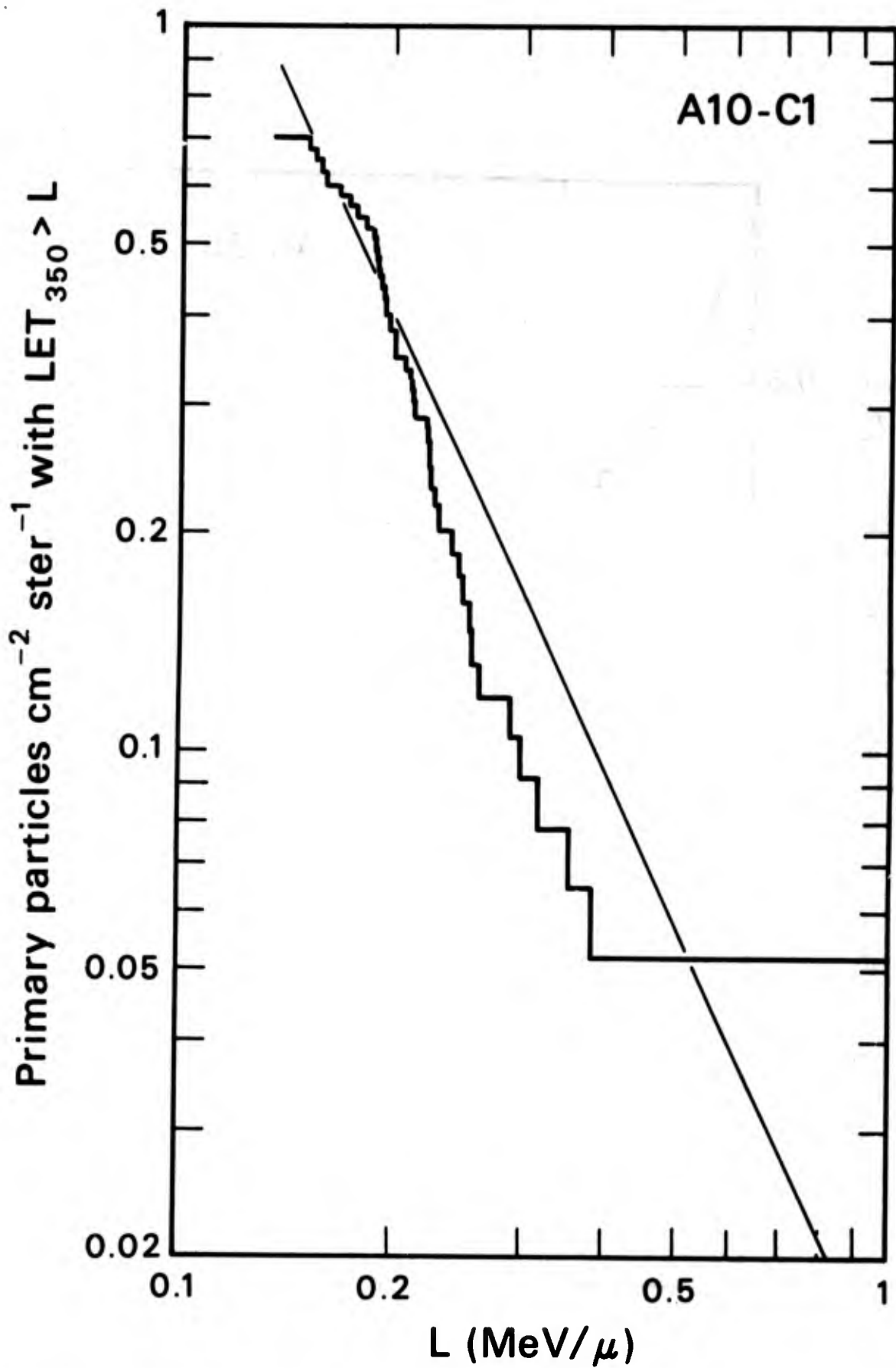the theoretical LET$_{350}$ spectrum is given by a straight diagonal line.

Figure 7. Measured integral LET$_{350}$ spectrum from Apollo 10 - C1. For comparison the theoretical LET$_{350}$ spectrum is given by a straight diagonal line.
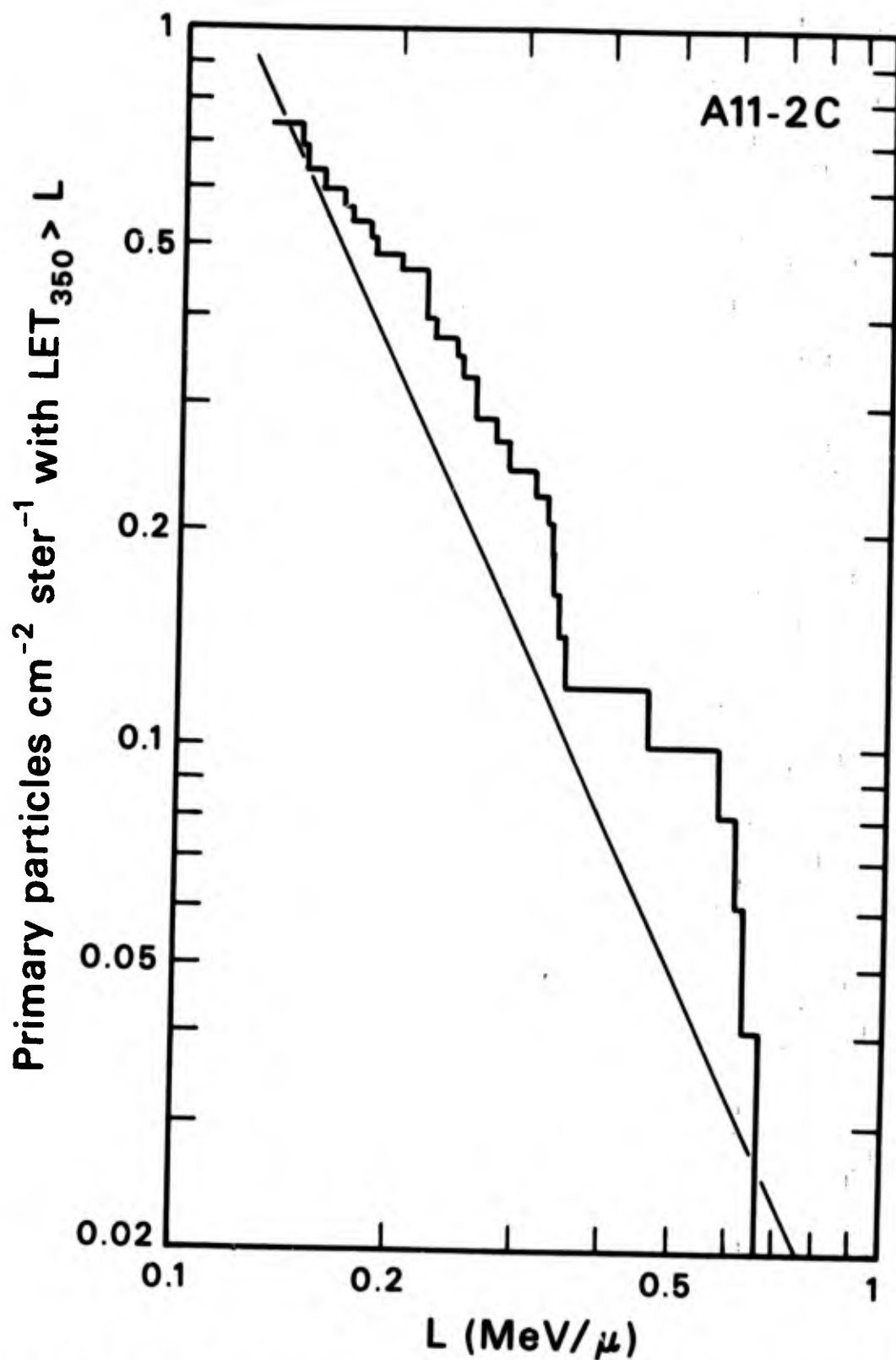
Figure 8. Measured integral LET$_{350}$ spectrum from Apollo 11 - 2C. For comparison the theoretical LET$_{350}$ spectrum is given by a straight diagonal line.
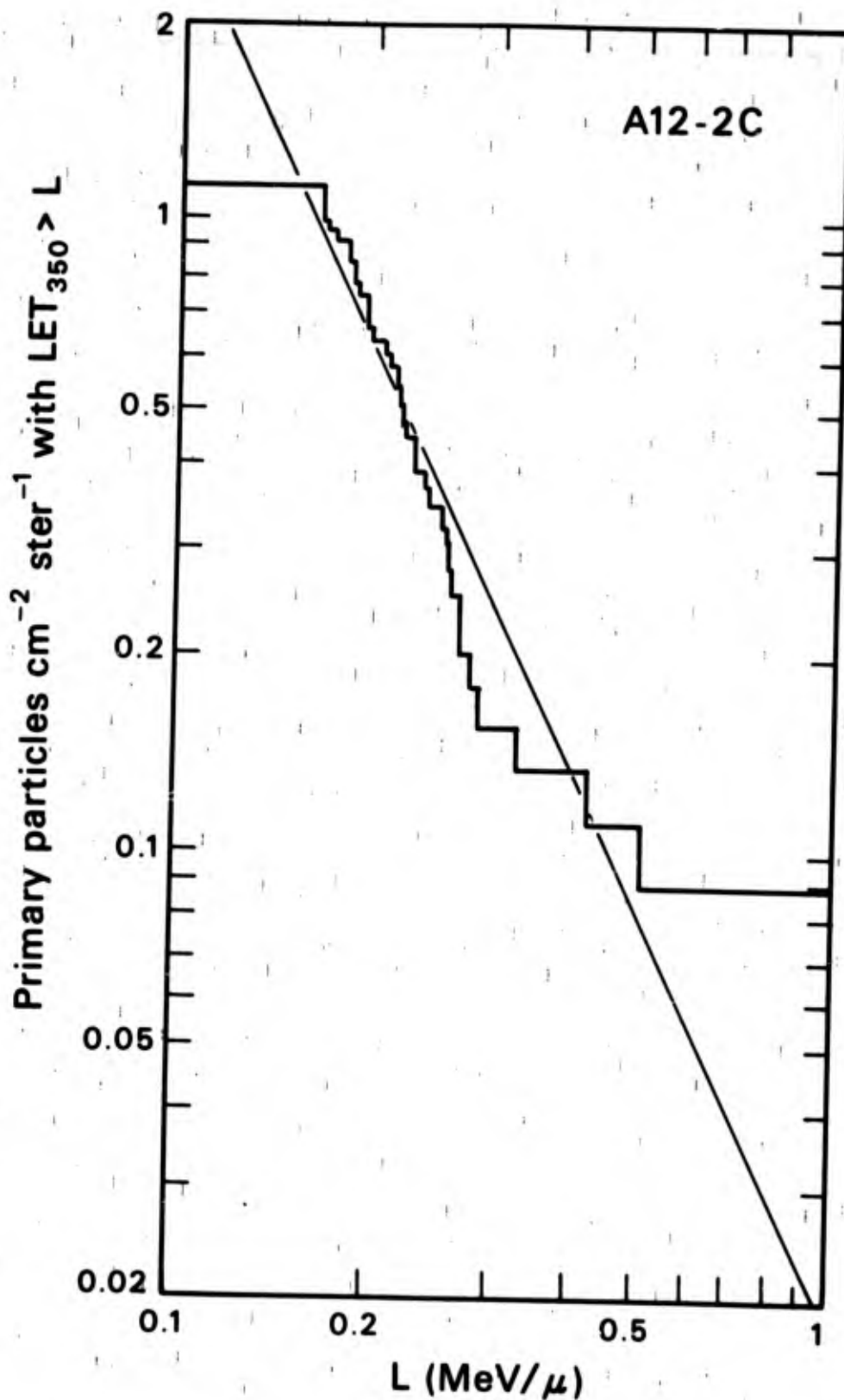
Figure 9. Measured integral LET$_{350}$ spectrum from Apollo 12 - 2C. For comparison the theoretical LET$_{350}$ spectrum is given by a straight diagonal line.

Figure 10. Measured integral LET_{350} spectrum from Apollo 13 - 3C. For comparison the theoretical LET_{350} spectrum is given by a straight diagonal line.
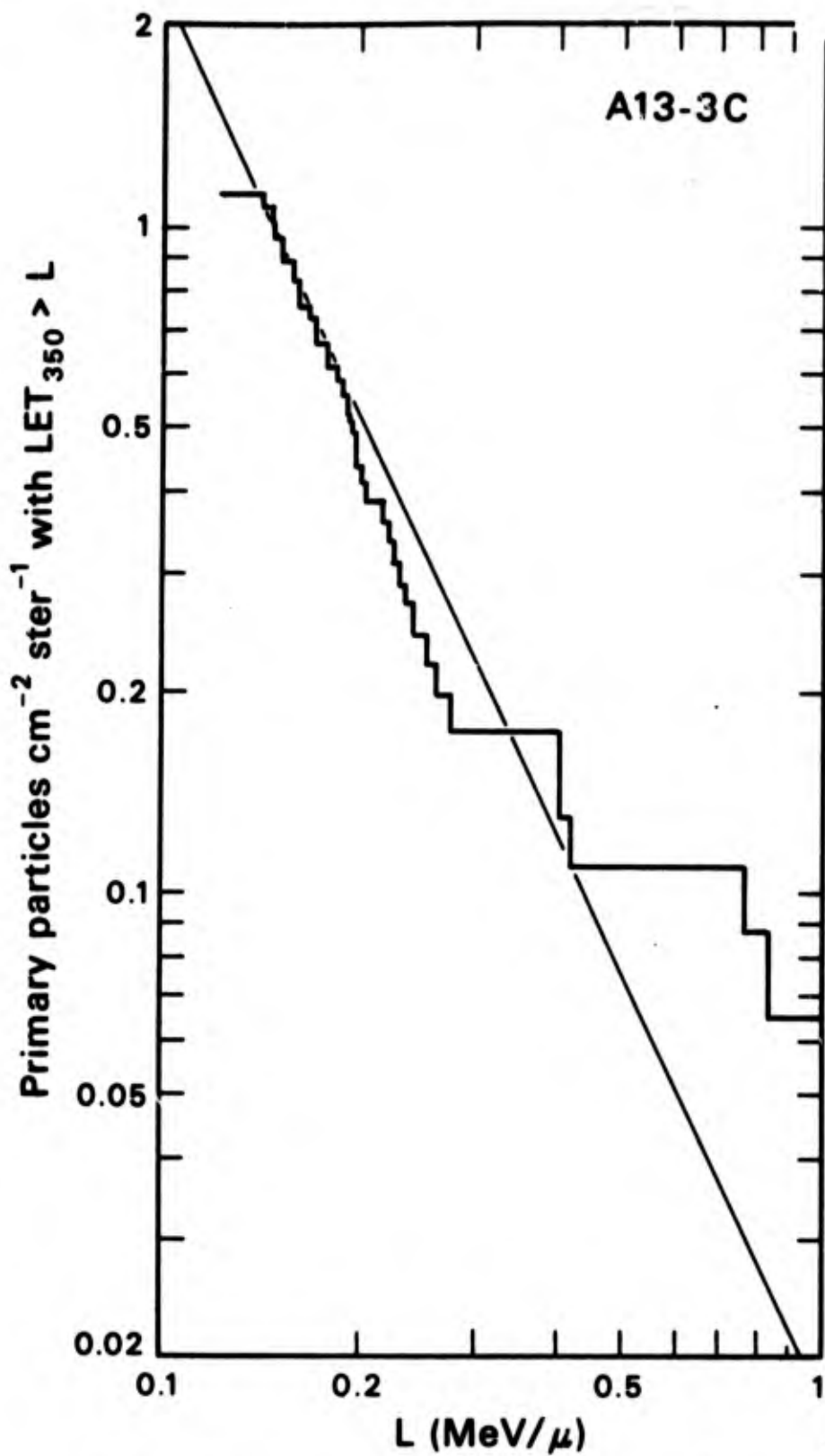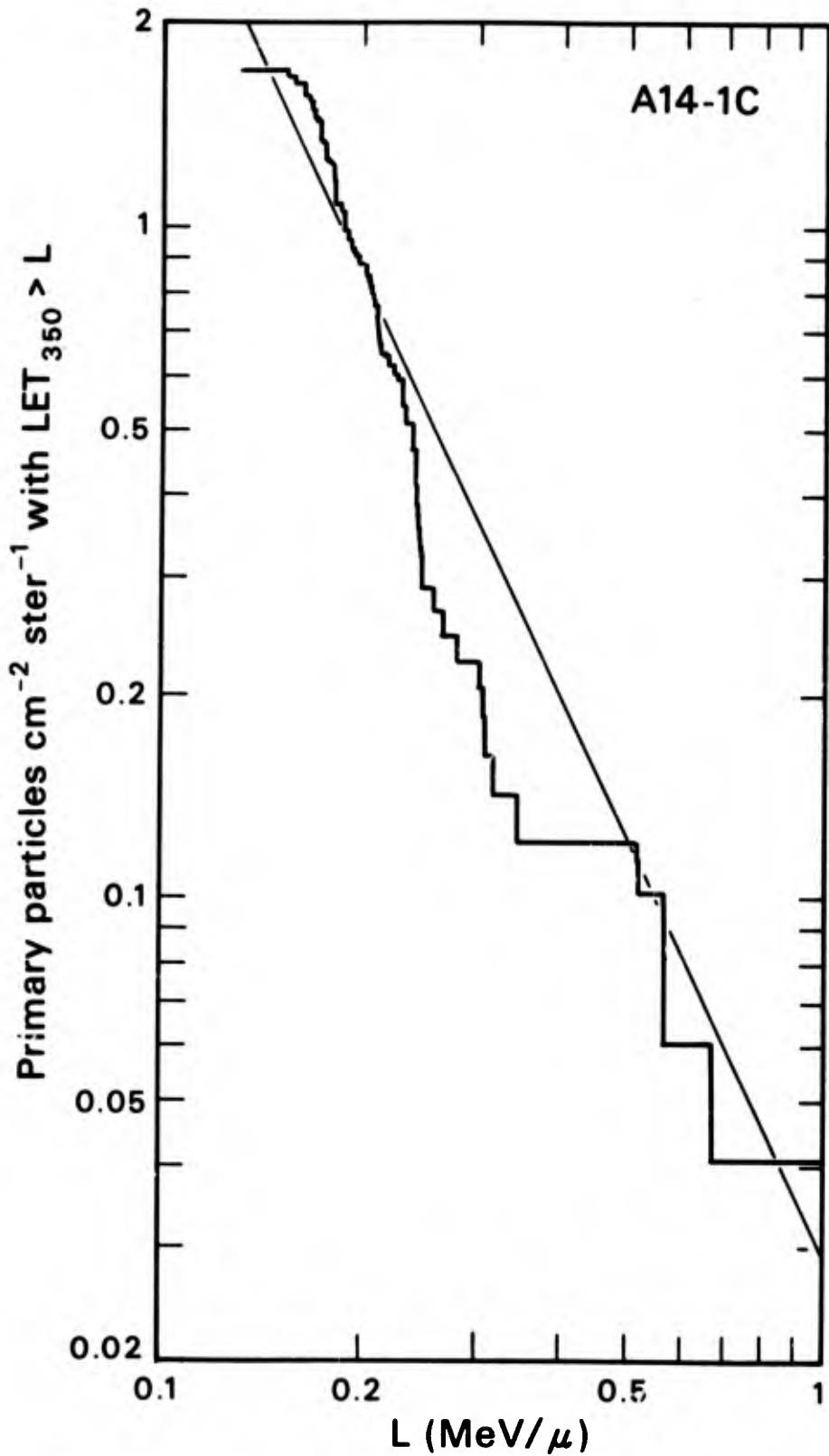
Figure 11. Measured integral LET$_{350}$ spectrum from Apollo 14. For comparison the theoretical LET$_{350}$ spectrum is given by a straight diagonal line.

$LET_\infty > L$ is given by

$$FCL \ (LET_\infty > L) = 4\pi \ 10^{-8} \int_L^\infty \frac{d^3N}{dA \ d\Omega \ dLET_\infty} \ \sigma_1 \ dLET_\infty$$

$$= 8.98 \times 10^{-5} \ C_L \int_L^\infty \sigma_1 \ LET^{-3.29} \ dLET_\infty \qquad (29)$$

The factor of 10^{-8} converts μ^2 to cm^2.

The FCL for each of the six Apollo flights is given in Figure 12 using the flight average value of C_L. The region of the plot with $L < 1$ is an extrapolation of the data based on the assumptio. of equal probabilities for all values of the residual range. Thus it includes only the low LET portion of the spectrum due to the $Z > 7$ particles which have been recorded at the higher LET ends of their trajectories. Lighter particles also contribute to the total FCL in this region but are not recorded by the Lexan detectors.
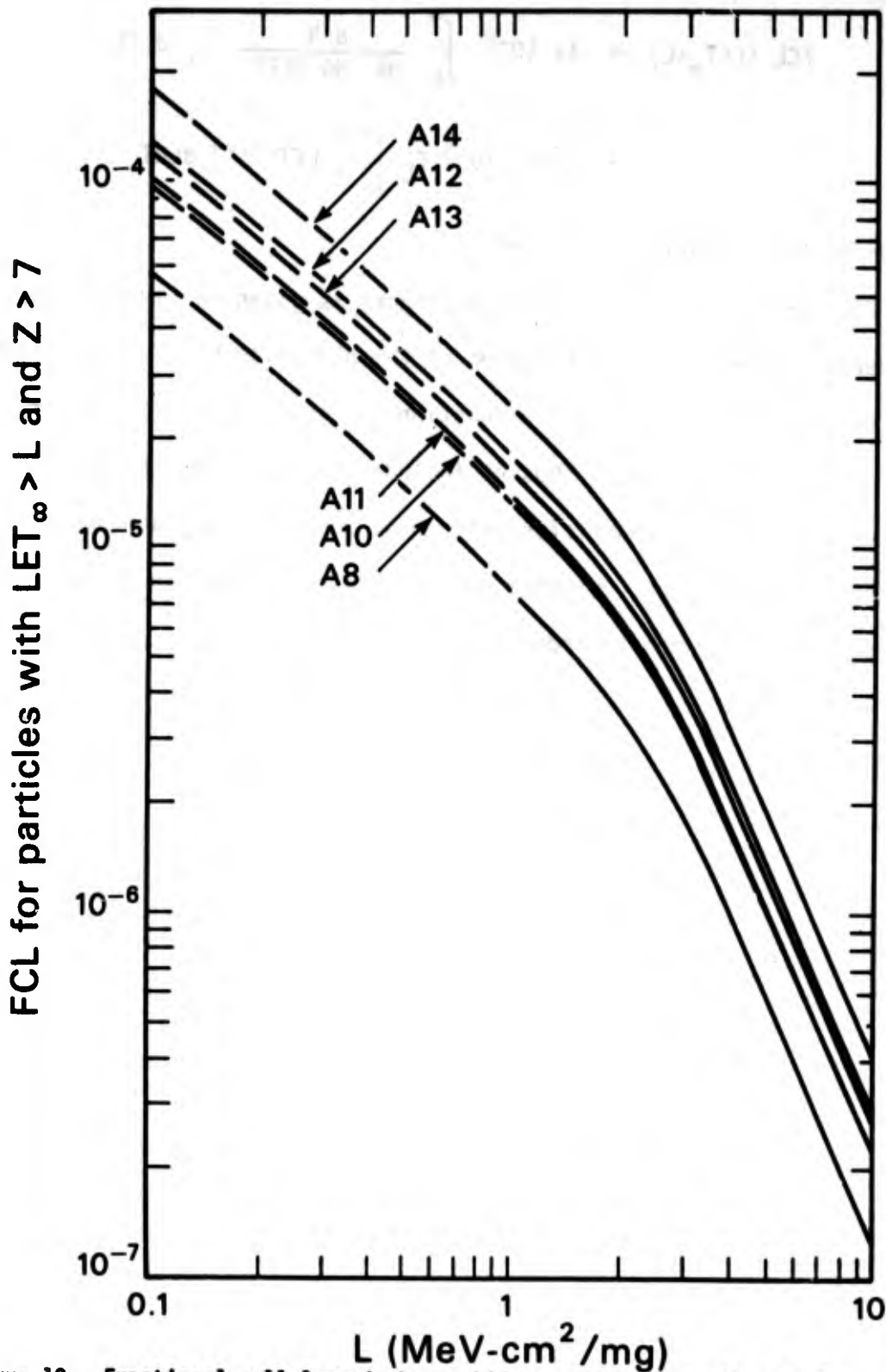
Figure 12. Fractional cell loss in human kidney cells due to the Z > 7, LET_{350} > L cosmic radiation particle component. The flight average curves for Apollo 8, 10, 11, 13, 12, and 14 are given respectively from bottom to top. The dashed lines for L < 1 MeV cm²/mg are extrapolations of the measurements based on the assumption that all values of the residual range are equally probable.

SECTION IV

DISCUSSION

The approach to data reduction in this paper differs somewhat from the approach used previously (Ref. 6). Previously, variations of the equation

$$R = C_R \, Z^\mu \, V_T^{-\lambda} \tag{30}$$

have been used in which λ or both μ and λ were assumed to be undetermined constants. For this report 3.29 and 1.00 are the adopted values of μ and λ. These values are quite consistent with the values that μ and λ assume when they are allowed to take on arbitrary values. With the value of μ and λ fixed, the total weight of the calibration measurement goes into determining C_R, producing a greater consistency in the results. Also, using $\lambda = 1$ simplifies the reduction equations somewhat.

Currently, several refinements of the reduction technique are being considered and developed. One of these is to improve the analytic representation of $LET(R,Z)$ and $V_T(LET)$. Previously the accuracy and completeness of the calibration data did not warrant more accuracy than a power function fit provides. However, improved accuracy and a greater range of the measured variables now provides the need for logarithmic polynomial approximations, the generalization of these power functions. Another area of development is the UV attenuation correction. Currently, the value of V_G used in the reduction formulae as given in this paper is the average bulk etch rate, which is an approximation to the bulk etch rate 1μ below the detector surface because of the relatively thin layer of detector surface removed. An improvement can be obtained by using a bulk etch rate as well as a track etch rate which has been corrected for UV attenuation. These corrected values would then be the same as if the entire

33

detector volume had received the same UV exposure as that received 1μ below the real detector's surface. The result of such a correction is expected to result in an increase of several per cent in the values of the $LET_{350} > 0.15$ MeV/μ fluences, the integral LET spectra, and the stopping densities.

The results presented in this paper should be compared with the observations of Comstock *et al.* (Ref. 7) of high Z particles in Lexan helmets of Apollo 8 and 12. By using a different processing technique that did not include a UV sensitization, and first using a replication technique of the interior surface, Comstock *et al.* (Ref. 7) measured 0.56 and 1.5 tracks/cm^2 in the Apollo 8 and 12 helmets, respectively. This compares with 2.6 and 5.0 tracks/cm^2 in Table III. The lower track fluences in the helmets correspond to the higher LET portion of the overall spectrum. It should be noted that the helmets are worn only a small fraction of the time and that the different helmets may be of slightly different sensitivity, and thus should be individually calibrated.

The errors that are indicated throughout this paper are the errors due to counting statistics alone. Other errors, such as those arising during the calibration and measuring processes, are not included because of the difficulty in assessing them. However in most cases these errors are smaller than those arising from the counting statistics.

The most interesting results and observations obtained to date with Lexan detectors can be summarized as follows:

1. Only the fraction of the $Z \gtrsim 10$ particle flux that corresponds to essentially stopping particles are recorded. These are the highest LET particles (and probably the most biologically significant) that either stop in the detector or the astronaut. For measurement of lower LET particles such as the $2 \leq Z \leq 9$ group or the more energetic $Z \gtrsim 10$ group, more sensitive detectors are required. Of the plastic detectors, cellulose triacetate, and cellulose nitrate have

34

sensitivities which fall in this range.

2. Comparison of track fluences measured on recent Apollo missions with those from earlier missions, indicates an increase in the high Z cosmic ray flux. This increase is partially due to a decrease in the degree of solar modulation.

3. Although the detectors are heavily biased toward the higher Z particles, fewer $Z = 26$ (Fe) particles are observed than expected as compared with lighter particles. This suggests a break-up of Fe particles in passage through the spacecraft shielding. Thus the Z spectrum inside the spacecraft is shifted toward the lighter particles.

4. Considerable variations have been found to exist in the recorded high Z track fluences as a function of detector location on the astronaut's body.

5. From these measurements, stopping particle densities in the form of integral Z distributions can be obtained.

6. High Z particle, integral LET spectra can be computed and therefore biologically meaningful quantities such as the fractional cell loss, FCL, can be obtained.

7. The frequency of the light flash phenomenon reported by the astronauts is considerably higher than the frequency with which the $LET_{350} \geq 0.15$ Mev/μ stopping particles are incident on tissue as recorded with Lexan. This implies that lower LET particles are at least partially responsible.

REFERENCES

1. R. P. Henke, E. V. Benton, H. H. Heckman, Radiation Effects, 3, 43 (1970).

2. R. P. Henke, E. V. Benton, "On Geometry of Tracks In Dielectric Nuclear Track Detectors," UCRL-20852.

3. E. V. Benton, "A Study of Charged Particle Tracks In Cellulose Nitrate," USNRDL-TR-68-14 (1968).

4. E. V. Benton, S. B. Curtis, R. P. Henke, C. A. Tobias, "Measurement of High-LET Particles On Biosatellite III," UCRL-20675 (1971).

5. E. V. Benton, R. P. Henke, "Heavy Cosmic-Ray Exposure of Apollo 14 Astronauts," USF-14, (1971).

6. P. Todd in Second Symposium On Protection Against Radiation In Space, NASA SP-71, 1964.

7. G. M. Comstock, R. L. Fleischer, W. R. Giard, H. R. Hart Jr., G. E. Nichols, P. B. Price, Science, 172, 154 (1971).